



Deposited via The University of Leeds.

White Rose Research Online URL for this paper:

<https://eprints.whiterose.ac.uk/id/eprint/105281/>

Version: Accepted Version

---

**Article:**

Boschmans, J, Jacobs, S, Williams, JP et al. (2016) Combining density functional theory (DFT) and collision cross-section (CCS) calculations to analyze the gas-phase behaviour of small molecules and their protonation site isomers. *Analyst*, 141 (13). pp. 4044-4054. ISSN: 0003-2654

<https://doi.org/10.1039/c5an02456k>

---

**Reuse**

Items deposited in White Rose Research Online are protected by copyright, with all rights reserved unless indicated otherwise. They may be downloaded and/or printed for private study, or other acts as permitted by national copyright laws. The publisher or other rights holders may allow further reproduction and re-use of the full text version. This is indicated by the licence information on the White Rose Research Online record for the item.

**Takedown**

If you consider content in White Rose Research Online to be in breach of UK law, please notify us by emailing [eprints@whiterose.ac.uk](mailto:eprints@whiterose.ac.uk) including the URL of the record and the reason for the withdrawal request.

# Combining density functional theory (DFT) and collision cross-section (CCS) calculations to analyze the gas-phase behaviour of small molecules and their protonation site isomers

Jasper Boschmans<sup>1</sup>, Sam Jacobs<sup>2</sup>, Jonathan P. Williams<sup>3</sup>, Martin Palmer<sup>3</sup>, Keith Richardson<sup>3</sup>, Kevin Giles<sup>3</sup>, Cris Laphorn<sup>4</sup>, Wouter A. Herrebout<sup>2</sup>, Filip Lemièrè<sup>1</sup>, Frank Sobott<sup>1,5,6</sup>

<sup>1</sup>*Biomolecular & Analytical Mass Spectrometry group, Department of Chemistry, University of Antwerp, Antwerp, Belgium,* <sup>2</sup>*Molecular Spectroscopy group, Department of Chemistry, University of Antwerp, Antwerp, Belgium,* <sup>3</sup>*Waters Corporation, Stamford Avenue, Wilmslow, SK9 4AX, UK,* <sup>4</sup>*Faculty of Engineering & Science, University of Greenwich, Medway Campus, Chatham, ME4 4TB, UK,* <sup>5</sup>*Astbury Centre for Structural Molecular Biology, University of Leeds, Leeds LS2 9JT, UK,* <sup>6</sup>*School of Molecular and Cellular Biology, University of Leeds, LS2 9JT, UK*

## **1. Abstract**

Electrospray ion mobility-mass spectrometry (IM-MS) data show that for some small molecules, two (or even more) ions with identical sum formula and mass, but distinct drift times are observed. In spite of showing their own unique and characteristic fragmentation spectra in MS/MS, no configurational or constitutional isomers are found to be present in solution. Instead the observation and separation of such ions appears to be inherent to their gas-phase behaviour during ion mobility experiments. The origin of multiple drift times is thought to be the result of protonation site isomers ('protomers'). Although some important properties of protomers have been highlighted by other studies, correlating the experimental collision cross-sections (CCS) with calculated values has proven to be a major difficulty. As a model, this study uses the pharmaceutical compound melphalan and a number of related molecules with alternative (gas-phase) protonation sites. Our study combines density functional theory (DFT) calculations with modified MobCal methods (e.g. nitrogen-based Trajectory Method algorithm) for the calculation of theoretical CCS

34 values. Calculated structures can be linked to experimentally observed signals, and a  
35 strong correlation is found between the difference of the calculated dipole moments of the  
36 protomer pairs and their experimental CCS separation.

37

38

39

## 40 **2. Introduction**

41

42 Ion mobility-mass spectrometry (IM-MS) is a separation and characterization technique  
43 that has proven to be applicable in many research fields since it started to gain popularity  
44 more than a decade ago with the introduction of the commercial Synapt system<sup>1</sup>. The drift  
45 time in ion mobility is determined by the collision cross-section (CCS) of an ion, which is a  
46 parameter related to its size, shape and charge. Originally used in structural studies  
47 investigating protein folding<sup>2-9</sup> and protein complexes<sup>10-15</sup>, more and more researchers  
48 are starting to use commercial IM-MS instrumentation to investigate the separation,  
49 identification and gas-phase behaviour of small molecules. A possible application is the  
50 rapid separation of all types of isomers, based on their mobilities (drift times)<sup>16-24</sup>.  
51 Recently, a number of ion mobility studies have reported on the observation of protomers  
52 for aniline and the antibacterial agent norfloxacin<sup>25-27</sup>. These isobaric ions are gas-phase  
53 protonation site isomers, where the protons are located on different atoms. Although the  
54 position of a single H atom and the positive charge appear to have a very subtle effect on  
55 these small molecules, they can cause clear differences in drift times. Such differences  
56 can be relatively large for small molecules, and one would therefore typically expect that  
57 they are due to the presence of isomers or conformers (i.e. size and shape differences).  
58 In a recent study, Warnke *et al.* used IM-MS in combination with infrared multiple photon  
59 dissociation (IRMPD) spectroscopy to study the origin of benzocaine protomers<sup>28</sup>.  
60 Differences in N-H and O-H stretch vibrations showed that two alternative sites are  
61 protonated: the amine and, unexpectedly, also the carbonyl group. These data confirm  
62 that the large difference between the observed CCS values for this compound is caused  
63 by the different charge sites, rather than e.g. the consequence of a subsequent  
64 gas-phase rearrangement reaction. The appearance of alternative gas-phase protonation  
65 sites highlights the possibility of intra-molecular charge transfer during the electrospray  
66 process<sup>28</sup>. Anionic species show similar phenomena, as was recently reported by  
67 Galaverna *et al.* for benzoic acid de-protomers<sup>29</sup>. It also questions the localization of

68 charges in multiply protonated peptide and protein ions, important for computational  
69 structure and fragmentation prediction, which are frequently assumed to remain on basic,  
70 surface-exposed residues such as lysine and arginine during the ESI process.  
71

72 Computational methods, such as molecular dynamics and quantum mechanical  
73 calculations, can support IM-MS observations (see Figure 1). These methods have  
74 become important tools for understanding and interpreting the experimental data, and  
75 they can potentially also be used to predict the separation of hypothetical charge isomers  
76 in ion mobility<sup>30,31</sup>. Interpretation of ion mobility data typically requires a conformational  
77 analysis of each protomer, after which all structures are optimized using DFT. This yields  
78 a set of geometries and associated partial atomic charges that can be used to compute  
79 the corresponding CCS values.

80 In this study we utilised the MobCal software<sup>32</sup>, which provides three different algorithms;  
81 the Projection Approximation (PA), Exact Hard Sphere Scattering (EHSS) and the  
82 Trajectory Method (TM). Of these, the most widely used are the PA and TM. In both the  
83 PA and EHSS methods the molecule is represented as a collection of overlapping hard  
84 spheres. The CCS calculated by the PA is simply the rotational average of the projected  
85 area of this collection. While fast, the PA fails to model momentum transfer between the  
86 gas and analyte molecules as well as concave analyte structure and long range ion  
87 molecule interactions. In the EHSS method, a full hard sphere trajectory is calculated for  
88 each analyte-gas collision. This is a significantly more sophisticated model, and it has  
89 found utility as a fast method for calculating CCS of large molecular structures<sup>33</sup>.  
90 Long-range interactions, which are often significant for drug-like molecules, are  
91 necessarily ignored. The TM is the most sophisticated and computationally intensive of  
92 the commonly used methods. It involves a simulation of the trajectory of gas atoms  
93 through a superposition of Lennard-Jones potentials corresponding to the atoms in the  
94 analyte molecule. Polarisation of the gas molecules by the charge on the analyte  
95 molecule is also taken into account, but modifications to the original algorithm are  
96 required to adequately model interactions with polyatomic gases. More recently, the  
97 Projected Superposition Approximation (PSA) algorithm was introduced by Bleiholder *et*.  
98 *al.*<sup>34-38</sup> In this approach, which is used mainly for larger molecules, the PA cross section is  
99 modified to take into account the detailed three-dimensional structure of the analyte.  
100 Although previous studies of protomers made use of methods originally available in  
101 MobCal, they were not always able to accurately reproduce the experimental CCS

102 values<sup>25,27</sup>. It is believed that IM-MS separations using polyatomic drift gases (such as N<sub>2</sub>  
103 or CO<sub>2</sub>) require a better representation of long-range interactions. The passage of a  
104 charged particle induces higher-order multipoles in the gas molecules, leading to  
105 additional (retarding) forces on the ion, and more collision geometries must be  
106 considered. Kim *et al.* proposed a modification to the existing trajectory method CCS  
107 calculation algorithms for N<sub>2</sub>, which takes ion-quadrupole interactions and the orientation  
108 of non-spherical gas molecules into account<sup>40,41</sup>. This modification leads to significantly  
109 higher calculated CCS values, which better conform to the experimentally determined  
110 data. Only a few studies have used this new approach so far to correctly reproduce  
111 experimental CCS values<sup>28,30,31,40-42</sup>. Apart from protomer-related studies, Lavanant *et al.*  
112 used the modified algorithm to calculate CCS values for phosphoric acid clusters, which  
113 can be used for negative ion mode IM calibrations<sup>43</sup>.

114  
115 The present study investigates 1. the experimental separation of hypothetical protomers  
116 for 7 related compounds which share an amino and carbonyl function (in aniline, a  
117 benzene ring) as alternative protonation sites; 2. the effect of using different levels of  
118 theory for optimization of molecular geometry and charge distribution, 3. the ability to  
119 obtain theoretical CCS that closely match experimental values; 4. the importance of the  
120 analyte charge distribution itself (and the resulting dipole moment) in contrast to possible  
121 charge-driven changes in molecular structure, and 5. the ability to predict protomer  
122 separation in ion mobility experiments based on the difference in the calculated molecular  
123 dipole moments for hypothetical protomer pairs. This study tests the hypothesis that  
124 experimentally found protomers can be predicted reasonably well by differences in the  
125 calculated dipole moments. The results reported here inform choices of computational  
126 approaches for the prediction of protomer separation in ion mobility so that spectral  
127 interpretation software (e.g. in metabolomics) could be trained to detect such  
128 phenomena.

129  
130

131

### 132 **3. Results and discussion**

133

#### 134 **3.1 IM-MS separation of protonation site isomers**

135 Two distinct peaks are observed in the arrival time distribution (ATD) of melphalan (*m/z*  
136 305) using nitrogen as drift gas: I' and I'' (see Figure 2), which are centred around 169.9

137 Å<sup>2</sup> and 179.1 Å<sup>2</sup>. However, for two other, closely related compounds,  
138 dimethoxymelphalan (DOCH<sub>3</sub>; II) and dihydroxymelphalan (DOH; III), we observe only  
139 single and unique peaks (Figure 2), at 172.2 Å<sup>2</sup> for DOCH<sub>3</sub> and 165.3 Å<sup>2</sup> for DOH. We  
140 also used CO<sub>2</sub> to perform ion mobility separations of DOCH<sub>3</sub> and DOH, but again only  
141 single peaks were observed (data not shown).

142 Similar observations to those with melphalan were made for the local anaesthetic  
143 *para*-benzocaine, an ethyl ester derivative of *para*-aminobenzoic acid (Figure 3). Two  
144 peaks were found (IV' and IV'') at 131.7 Å<sup>2</sup> and 147.5 Å<sup>2</sup>. For comparison, positional  
145 isomers of benzocaine were also studied (Figure 3): ethyl 2-aminobenzoate  
146 (“*ortho*-benzocaine”) and ethyl 3-aminobenzoate (“*meta*-benzocaine”). The selected-ion  
147 ATD of *ortho*-benzocaine shows only one peak at 135.2 Å<sup>2</sup> (V). For *meta*-benzocaine, two  
148 peaks are observed (VI' and VI'') which correspond to CCS values of 133.6 Å<sup>2</sup> and 146.4  
149 Å<sup>2</sup>. For aniline, which we included here as a reference compound, we find two peaks as  
150 reported previously<sup>25</sup> (VII' and VII''); see Figure 3), with CCS values of 112.9 Å<sup>2</sup> and 118.9  
151 Å<sup>2</sup>. Table 1 summarizes all experimental CCS values.

152

### 153 3.2 Calculating CCS values of melphalan protomers

154 Three possible protomers of melphalan were taken into account here: protonation at the  
155 nitrogen atom of the NH<sub>2</sub> group (N<sub>AA</sub>), the carboxyl group (O<sub>CO</sub>) on the amino acid side,  
156 and the nitrogen atom adjacent to the phenyl ring on the chloroethyl side (N<sub>Cl</sub>). Based on  
157 the solution basicity (i.e. pK<sub>a</sub>) of the various functional groups in melphalan<sup>44</sup>, O<sub>CO</sub> and N<sub>Cl</sub>  
158 protonation seem less plausible (see Figure 2). Nonetheless, other protomer studies  
159 have reported on oxygen-rich functional groups or even aromatic rings<sup>25-28</sup> as preferred  
160 protonation sites. After performing a conformational analysis of melphalan and  
161 subsequent DFT optimisation at the B3LYP/6-31G(d,p) level (hereafter referred to as  
162 “standard” level), the CCS values for the optimised structures were calculated using a  
163 modified version of MobCal where the TM code optimized for use with nitrogen (see  
164 Figure 1). Table 2 gives an overview of the top 5 lowest-energy conformers of each  
165 melphalan protomer, together with energies, overall Boltzmann weights, dipole moments  
166 and calculated CCS values. Figure 4 visualizes the conformation and molecular  
167 electrostatic potential (MEP) of each lowest-energy melphalan protomer.

168 From the three protomers considered here, the N<sub>AA</sub> and N<sub>Cl</sub> forms best match the  
169 experimentally determined CCS<sub>N<sub>2</sub></sub>. This would indicate that the O<sub>CO</sub> protomer is not  
170 observed during the ion mobility experiments. The ΔCCS<sub>N<sub>2</sub></sub> between the calculated N<sub>AA</sub>

171 and  $N_{Cl}$  protomers is  $9.0 \text{ \AA}^2$ , which is a good match with the experimentally determined  
172 value of  $9.2 \text{ \AA}^2$ .

173

### 174 3.3 Melphalan-related compounds: dihydroxymelphalan and dimethoxymelphalan

175 The study of melphalan derivatives, which unlike melphalan itself show only one  
176 observed drift time, allows us to investigate the factors that govern formation and  
177 separation of melphalan protomers more closely. A conformational analysis was  
178 performed for possible protomers of these compounds, and the resulting structures were  
179 optimised at “standard” level. Although DOH and  $DOCH_3$  are chemically less complex  
180 structures than melphalan itself (i.e. no halogen atoms), the additional rotational flexibility  
181 yields more conformers and thus entails an added computational cost. For each  
182 lowest-energy protomer, the values are reported in Table 3 and structures are given in  
183 Figure 2. Calculated CCS values were also compared to the experimentally derived ones  
184 ( $172.2 \text{ \AA}^2$  for  $DOCH_3$  and  $165.3 \text{ \AA}^2$  for DOH). This allows us to evaluate the  
185 nitrogen-modified MobCal code, but could also show whether significantly different CCS  
186 values are calculated for protomers in cases where they are not experimentally resolved.  
187 The  $N_{AA}$  protomer for DOH has a considerably smaller calculated CCS ( $156.1 \text{ \AA}^2$ ) than the  
188 experimentally observed value. The CCS of the  $N_{OH}$  protomer on the other hand ( $164.6$   
189  $\text{ \AA}^2$ ) is a close match with the experiment. For  $DOCH_3$ , the calculated CCS values of both  
190 hypothetical protomers ( $181.3 \text{ \AA}^2$  and  $182.3 \text{ \AA}^2$ ) over-estimate the experimental CCS of  
191  $172.2 \text{ \AA}^2$ .

192

### 193 3.4 Other related small molecules: benzocaine isomers and aniline

194 Our calculation strategy was further evaluated against experimentally determined CCS  
195 values of benzocaine isomers and aniline (Table 4). For *para*-benzocaine, protonation of  
196 the carbonyl group gives a  $CCS_{N_2}$  of  $132.0 \text{ \AA}^2$  for the lowest-energy structure after  
197 standard-level optimization, while the equivalent procedure for the amine-protonated  
198 species results in a  $CCS_{N_2}$  value of  $140.9 \text{ \AA}^2$ , which is significantly smaller than the  
199 experimental value ( $147.5 \text{ \AA}^2$ ). While the theory correctly predicts the separation of the  
200 two protomers, it remains unclear why the calculated value for the amine-protonated  
201 *para*-benzocaine deviates so much from the experiment.

202 After standard-level optimization,  $O_{CO}$  and  $N_{NH_2}$  protomers of *ortho*-benzocaine have  
203 computed CCS values of  $131.0$  and  $131.5 \text{ \AA}^2$ , respectively. Based on these values,  
204 assignment of the single experimentally observed peak to either protomer is difficult, as

205 they are expected to be almost indistinguishable. It is therefore impossible to say whether  
206 they both occur in the gas phase, with their peaks overlapping, or if only one of them is  
207 present. In this context it is worth noting that a recent report proposed the two alternative  
208 forms of deprotonated *ortho*-hydroxybenzoic acid to be connected by a relatively low  
209 isomerization barrier<sup>29</sup>. It might therefore be considered likely that the protomers of  
210 *ortho*-benzocaine could also easily convert due to intramolecular H-bonding, leading to  
211 only one mobility signal.

212 Two distinct CCS values are calculated after standard-level optimization for  
213 *meta*-benzocaine: 133.9 Å<sup>2</sup> for the O<sub>CO</sub> isomer and 140.8 Å<sup>2</sup> for the N<sub>NH2</sub> protomer. While  
214 such calculations predict reasonably well if the postulated protomers will be separated by  
215 ion mobility (one or two peaks expected), the absolute CCS values do not always match  
216 well with the measured ones, e.g. for the N<sub>NH2</sub> form of *meta*-benzocaine.

217 The calculated CCS value of the N protomer of aniline (at “standard” level) is also not well  
218 matched with either of the experimental values (112.9 Å<sup>2</sup> and 118.0 Å<sup>2</sup>). The  
219 ring-protonated species should be assigned to the first peak in the ATD, based on data  
220 reported in the literature<sup>25</sup>.

221

### 222 3.5 Evaluating different levels of DFT calculations

223 Although the majority of ion mobility studies employ the commonly used B3LYP functional  
224 with 6-31G or 6-311G basis sets, a wide variety of other functionals and basis sets are  
225 available. Because the CCS values computed so far, using the “standard” level combined  
226 with the N<sub>2</sub>-modified MobCal code, still show some discrepancies with the experiment, we  
227 also used B3PW91/def2-TVZP (hereafter called “high” level) in order to assess how  
228 sensitive the computed values are to the DFT parameters. Tables 1, 3 and 4 and Figures  
229 S.2 to S.9 contrast “standard” with high-level calculated CCS values.

230 For the benzocaine isomers and aniline, we found that the high-level calculations yield  
231 generally better matches against the experimental values (Table 1).

232 Both postulated protomers of DOH are found to have similar CCS at “high” level, which  
233 also closely match the single observed peak centred at 165.3 Å<sup>2</sup>. The “standard” level  
234 result, where the CCS value for the N<sub>AA</sub> protomer was underestimated (156.1 Å<sup>2</sup>), falsely  
235 suggested that two distinct DOH protomers should exist, with a  $\Delta\text{CCS}_{\text{N}_2}$  of 8.5 Å<sup>2</sup> (Table  
236 3).

237 For the DOCH<sub>3</sub> form of melphalan on the other hand, the CCS values calculated at both  
238 levels of structural optimization (around 180 Å<sup>2</sup>) are significantly higher than the

239 measured one (172.2 Å<sup>2</sup>). It is not apparent though why CCS calculations for this  
240 compound deviate so much from the experiment.

241 For melphalan itself, the expected improvement in the theoretical values is also less  
242 pronounced when using the B3PW91 functional and larger basis set. Notably the CCS of  
243 the N<sub>Cl</sub> protomer is now overestimated: 170.6 Å<sup>2</sup> (“standard” level) vs. 174.1 Å<sup>2</sup> (“high”  
244 level). Since the experimentally derived value for this protomer is 169.9 Å<sup>2</sup>, the “standard”  
245 level result is in better agreement in this particular case. While the reason for this anomaly  
246 is not entirely clear, melphalan stands out as a compound with the highest conformational  
247 “flexibility” (see below) in the group studied here.

248 We show here that for a number of structurally related compounds, the calculation of  
249 “best” molecular geometries and charge distributions using two different levels of DFT  
250 calculations leads to mixed results, with respect to how well the derived CCS match with  
251 experimentally observed CCS (see Figure 5). Contrary to what we might have expected,  
252 the high-level calculations do not always agree better with experiment. A more thorough  
253 investigation of different basis sets and functionals is needed, as well as a  
254 re-parametrization of CCS calculation methods, which currently rely on modifications to  
255 the existing MobCal code. Such efforts are now underway in different research groups.

256

### 257 3.6 Effect of charge distribution on CCS calculations

258 Although this study assumes that different protonation site isomers can be formed in the  
259 electrospray process and observed via their characteristic mobility peaks, the question  
260 still remains to what extent different factors contribute to protomer separation in ion  
261 mobility: is it the charge site itself, or rather the conformational change driven by  
262 alternative charge sites? As an example of the latter, the rotation of the chloroethyl  
263 groups in the mustard moiety of melphalan could lead to the observation of multiple  
264 conformers. Interaction of these chloroethyl groups with the phenylalanine moiety of the  
265 molecule could possibly also result in more compact ions.

266 Protonation at different sites, which results in different charge distributions (after  
267 optimization) across the molecule, can potentially affect its geometry (i.e. the atomic  
268 positions) in a way that contributes to a change in CCS. In order to assess the magnitude  
269 of this effect separately from that of the charge distribution itself, we simply recalculated  
270 the CCS, while removing the atomic partial charges. These re-calculated CCS values are  
271 reported in **Table 5** (“no charge distribution”). Removing the charges drastically lowers the  
272 computed CCS values, as expected in N<sub>2</sub> drift gas particularly for the smaller analytes

273 (benzocaine isomers and aniline), and we do not expect them to match the experimental  
274 values anymore. More importantly, what this exercise can show is if the calculated CCS  
275 difference between two postulated protomers is maintained even in the absence of any  
276 charge, i.e. whether it is largely caused by a conformational change of the molecule. This  
277 is the case only for the melphalan protomers. All other molecules studied here show  
278 virtually identical CCS (within the error margin of the experiment) for the “uncharged”  
279 protomer pairs. This signifies that the potentially different molecular geometries of the  
280 protomers, optimised in the presence of charge, would not account for any possible CCS  
281 difference. Rather the position of the proton and the resulting relatively large differences  
282 in charge distributions and dipole moments are held responsible for the observed  
283 protomer separation in ion mobility. We can speculate that of the molecules studied here,  
284 only melphalan is “flexible” enough to undergo a charge-site driven conformational  
285 change which is sufficiently large to contribute to the separation of its protomer peaks.  
286 These calculations show that different protonation sites can yield significantly different ion  
287 mobilities in nitrogen, indicating that the long-range electrostatic contribution of the  
288 charge to the overall CCS is substantial.

289

### 290 3.7 Protomers and dipole moments

291 The analysis of the effect of molecular geometry on CCS independent of charge (see  
292 section 3.6) showed that for some of the small molecules studied here, charge  
293 distributions are the determining factor for their separation in ion mobility when using  
294 polarizable gases. A close look at the structures of the protomer pairs shows that,  
295 although their mobilities can differ considerably, their geometries may indeed be relatively  
296 similar. Since the atomic coordinates of these structures only vary slightly (apart from  
297 melphalan), the CCS difference is thought to be predominantly the result of the charge  
298 distribution. The differences between the molecular dipole moment of various protomers  
299 could therefore be used as a possible predictor for the separation of these protomers in  
300 ion mobility<sup>30</sup>.

301 As an example, the charge distributions of the three melphalan protomers considered  
302 here are visualized as molecular electrostatic potentials (MEPs) in Figure 4. Comparison  
303 of the 5 lowest-energy structures per protonation site (see Table 2) shows that they share  
304 similar dipole moments. Furthermore, the structures with the smallest dipole moment (ca.  
305 6 Debye) also correspond to the ion with the smallest CCS value, i.e. the N<sub>Cl</sub> protomer.  
306 The structures that have a dipole moment of around 11 Debye correspond to the ion with

307 the largest observed CCS value ( $N_{AA}$  protomer). We plotted all 4 experimentally observed  
308 protomer pairs with their  $\Delta CCS$  values against the corresponding Delta dipole values,  
309 calculated at the best-fitting DFT level (apart from melphalan, all “high” level; see Figure  
310 6). Although the correlation is not very strong, the trend is clear: the larger the calculated  
311 Delta dipole values, the higher the measured Delta CCS.

312 To test this hypothesis further, we also plotted predicted  $\Delta CCS$  values for all possible  
313 protomer pairs, calculated at both “standard” and “high” levels using MobCal, against  
314 their corresponding Delta dipole values. These data highlight that the correlation between  
315 CCS and dipole moment is quite poor with standard-level calculations (red squares in  
316 Figure 6). The high-level structure calculations on the other hand (blue diamonds) yield a  
317 reasonably good correlation (linear fit:  $R^2=0.8784$ ) between differences in dipole moment  
318 of protomer pairs and their separation in ion mobility experiments where polarisable drift  
319 gases such as nitrogen are used<sup>30,31</sup>. Aniline shows a  $\Delta CCS$  larger than expected based  
320 on the calculated  $\Delta$  dipole value, which may be due to the fact that the smaller protomer is  
321 a ring-protonated (charge-delocalized) form.

322 Taken together, these data suggest that rather than geometry or net charge alone, the  
323 charge distribution – characterized by the dipole moment and, as recently proposed<sup>29</sup>, the  
324 polarizability of the analyte – plays a major role for the observed CCS values as well,  
325 particularly for relatively rigid molecules and their specific interaction with a polarizable  
326 drift gas (i.e.  $N_2$ ). Experimentally observed protomer separation is found to be explained  
327 reasonably well by differences between the calculated dipole moments of alternatively  
328 protonated forms of the analyte.

329

330

331

## 332 **4. Experimental**

333

334 Caution: melphalan and degradation products are carcinogenic and should be handled  
335 with care.

336

### 337 **4.1. Chemicals and sample preparation**

338 Chemicals purchased from Sigma-Aldrich (Bornem, Belgium): acetaminophen (> 99.0  
339 %), alprenolol (Eur. Pharmacop. Ref.), aniline (99.8 %), colchicine (> 95 %),  
340 dexamethasone (> 97 %), ethyl 4-aminobenzoate (98 %), ethyl 3-aminobenzoate (97 %),

341 ethyl 2-aminonbenzoate (> 99 %), N-ethylaniline (98 %), melphalan (min. 95 %),  
342 ondansetron (> 98 %), poly-DL-alanine, sodium formate (HPLC, > 99.0 %) and verapamil  
343 (> 99 %). Acetonitrile (ACN; HPLC grade), methanol (MeOH; HPLC grade) and formic  
344 acid (FA; 99+ %) were obtained from Acros (Geel, Belgium). Reversed osmosis (RO)  
345 water was prepared using a Silex water filtering system from Eurowater (Nazareth-Eke,  
346 Belgium). Ammonium hydroxide (solution of 25 % v/v) was purchased from Merck  
347 (Overijse, Belgium). Dimethoxymelphalan was synthesized in-house, and  
348 dihydroxymelphalan formed during synthesis as an additional reaction product. Stock  
349 solutions ( $10^{-2}$  M) of all analytes and calibrants were prepared in MeOH.

350

#### 351 4.2 Optimisation of molecular structures and charge distributions

352 A conformational analysis was performed to find the best structure of melphalan ions in  
353 the gas phase. The conformational space of the different protonated species  
354 ('protomers') was explored using TINKER (version 6)<sup>45</sup> with the Merck molecular force  
355 field (MMFF94). The resulting structures were further optimised with Gaussian 09<sup>46</sup> at the  
356 B3LYP/6-31G(d,p) ("standard") and B3PW91/def2-TZVP ("high") levels. For each  
357 calculation, the optimised structure was verified to be a local minimum by performing a  
358 vibrational analysis. Atomic charges were computed using the Merz-Singh-Kollman  
359 scheme with the constraint to reproduce the molecular dipole ('pop=mk,dipole'). The  
360 uncharged structures were generated by simply removing the atomic partial charges. As  
361 the dipole moment for charged species depends on the origin chosen, the center of  
362 charge was used as a reference point instead of the center of mass for all calculations.  
363 Three-dimensional structures were visualized using Avogadro (version 1.1.1)<sup>47</sup> and  
364 molecular electrostatic potentials (MEPs) using VMD (version 1.9.2)<sup>48,49</sup>.

365

#### 366 4.3 Calculation of CCS values

367 MobCal was used to calculate CCS values<sup>32,33</sup>. MobCal is available as freeware<sup>50</sup>.  
368 MobCalPARSER, also available as freeware<sup>51</sup>, allowed the direct use of Gaussian output  
369 (.log) files.

370 The modified version of MobCal<sup>41</sup> used in this study calculates CCS values for  
371 experiments in nitrogen drift gas and takes into account ion-quadrupole interactions and  
372 the orientation of non-spherical gases during collisions (TM algorithm only).  
373 Lennard-Jones potentials were re-tuned by scaling universal force field (UFF) parameters  
374 such as the atomic energy and van-der-Waals distance, in order to represent the ion

375 motion through N<sub>2</sub> drift gas better. The code was also expanded with other types of  
376 atoms.

377

#### 378 4.4 Instrumentation

379 Travelling-Wave Ion Mobility Spectrometry (TWIMS) experiments were performed on a  
380 Synapt G2 HDMS instrument, and data acquisition and processing were carried out using  
381 MassLynx (V 4.1).

382 The instrument (Waters Corporation, Wilmslow, UK) was equipped with a  
383 nano-electrospray source and used gold-coated glass capillary needles, which were  
384 fabricated in-house. In order to obtain clean spectra, the ions under investigation were  
385 *m/z* selected in all IM-MS experiments. Prior to the experiments, the instrument was  
386 calibrated in the *m/z* 50-600 mass range using sodium formate solution (positive ion  
387 mode). All prepared solutions were checked for the presence of impurities, which might  
388 overlap with the signal of the analyte.

389 Typical instrument parameters in time-of-flight mode are: sample and extraction cone  
390 voltage: 10 V and 3 V, trap bias: 2 V, trap cell gas flow: 2 mL/min, trap and transfer CE: 4  
391 V and 0 V. Experimental CCS are determined after a single calibration of the TWIMS cell  
392 using both poly-DL-alanine (0.5 mg/mL in 1:1 H<sub>2</sub>O:ACN) and a set of drug-like  
393 compounds (5 μM each in 1:1 H<sub>2</sub>O:ACN) as reported before<sup>12,39</sup>. In ion mobility mode,  
394 drift times were determined for different IM wave velocities in order to eliminate  
395 energy-dependent phenomena, which could affect the ion mobility separation. Some  
396 parameters differ in ion mobility mode: trap bias: 40 V, IMS wave velocity: 600 m/s or, for  
397 melphalan and related compounds: 1000 m/s, IMS wave height: 40 V, He and IMS  
398 (nitrogen) gas flow: 180 mL/min and 90 mL/min.

399

400

401

#### 402 5. Conclusions

403

404 Most small compounds show only one, unique drift time in ion mobility experiments, which  
405 allows the use of such data as additional identifiers for mass-spectrometry based  
406 molecular characterization, e.g. in metabolomics. There is now considerable interest in  
407 assembling databases which contain ion mobilities of compounds under standardized  
408 conditions, not dissimilar to retention times in chromatography.

409 Occasionally, small molecules exhibit multiple ion mobility drift times, due to the ability to  
410 form different protomers. Protomers are constitutional isomers, or more precisely,  
411 isomeric cationomers. They are molecular species which originate from the same chemical  
412 entity in solution, but where partial, intramolecular proton transfer during electrospray  
413 ionization causes the formation of charge isomers in the gas phase. This is often  
414 encountered for, but not limited to, small molecules containing an amino and a carbonyl  
415 or carboxyl moiety. Protonation at different sites may not only distort the molecular  
416 geometry, affecting the hard sphere cross-sections, but also lead to significantly different  
417 charge distributions. The latter can be represented by the dipole moment, which has a  
418 large effect on the ion's mobility when polarisable drift gases such as nitrogen are used.

419  
420 In the most systematic analysis to date, we utilized a panel of 7 closely related small  
421 molecules, 4 of which are found to show two drift time signals, to better understand what  
422 determines protomer separation in ion mobility and evaluate computational approaches  
423 for their characterization. IM-MS of the chemotherapeutic agent melphalan revealed the  
424 presence of two mobility peaks, whereas molecules closely related to this compound (i.e.  
425 dihydroxy- and dimethoxymelphalan) only showed one protonated form. For comparison,  
426 aniline and three isomers of benzocaine were also included in this study.

427 By comparing experimental with calculated CCS values from molecular modelling, we  
428 could assign the protonation site and structure of the observed ions. More flexible  
429 structures with bulky side chains (e.g. DOCH<sub>3</sub>) however appear to have their CCS  
430 overestimated with both types of calculations used. While results of what we call  
431 “high-level” calculations match experimental data much better for most molecules studied  
432 here, a more systematic investigation of functionals and basis sets is required to  
433 determine the most appropriate computational strategy for the optimization of structure  
434 and charge of protomers. With different protonation sites in these compounds available  
435 under electrospray conditions, a number of alternative charge distributions and molecular  
436 geometries have to be evaluated for how well they match the corresponding collision  
437 cross sections in the experiment. More straightforward and efficient calculation methods  
438 would make this step much faster and more accurate, and enable “high-throughput”  
439 approaches for ion mobility data processing such as would benefit, e.g., compound  
440 identification in complex samples.

441 The use of polarisable drift gases (e.g. N<sub>2</sub>), which has become common due to the  
442 widespread use of travelling wave IM-MS, leads to a more frequent observation of

443 protomer phenomena, and puts the issue of their structural assignment into the spotlight.  
444 We found a good agreement between experimental and theoretical CCS data in this  
445 study when using a modified version of the trajectory method, optimised for use with  
446 nitrogen as drift gas. Our data show that the molecular dipole moment, rather than the  
447 hard sphere collision cross section, is a useful determinant for the ion mobility separation  
448 of protomers. Furthermore, a good correlation appears to exist between the different  
449 calculated dipole moments, and both experimental and theoretical CCS differences, in  
450 protomer pairs investigated here. As calculated dipole moments are readily available,  
451 they may be useful “predictors” of protomer separation in experiments which target rapid  
452 small molecule isomer separation and identification using ion mobility.

453

454

455

#### 456 **Acknowledgements**

457

458 Financial support by the Hercules Foundation Flanders allowing the purchase of the  
459 Synapt instrument and the CalcUA/VSC supercomputing cluster is acknowledged. We  
460 thank Iain Campuzano (Amgen, Thousand Oaks, CA, USA) for providing us with the  
461 modified MobCal algorithm and helpful discussions, and wish to thank the reviewers for  
462 their constructive feedback.

463

464

465

#### 466 **References**

467

- 468 1. K. Giles, S. D. Pringle, K. R. Worthington, D. Little, J. L. Wildgoose and R. H. Bateman,  
469 *Rapid Comm. Mass Spectrom.*, 2004, **18**, 2401-2414.
- 470 2. K. Thalassinos, S. E. Slade, K. R. Jennings, J. H. Scrivens, K. Giles, J. Wildgoose, J.  
471 Hoyes, R. H. Bateman and M. T. Bowers, *Int. J. Mass Spectrom.*, 2004, **236**, 55-63.
- 472 3. H. A. Sawyer, J. T. Marini, E. G. Stone, B. T. Ruotolo, K. J. Gillig and D. H. Russell, *J. Am.*  
473 *Soc. Mass Spectrom.*, 2005, **16**, 893-905.
- 474 4. S. D. Pringle, K. Giles, J. L. Wildgoose, J. P. Williams, S. E. Slade, K. Thalassinos, R. H.  
475 Bateman, M. T. Bowers and J. H. Scrivens, *Int. J. Mass Spectrom.*, 2007, **261**, 1-12.
- 476 5. C. A. Scarff, K. Thalassinos, G. R. Hilton and J. H. Scrivens, *Rapid Commun. Mass*  
477 *Spectrom.*, 2008, **22**, 3297-3304 .

- 478 6. D. P. Smith, T. W. Knapman, I. Campuzano, R. W. Malham, J. T. Berryman, S. E. Radford  
479 and A. E. Ashcroft, *Eur. J. Mass Spectrom.*, 2009, **15**, 113-130.
- 480 7. C. W. N. Damen, Chen, A. B. Chakraborty, M. van Oosterhout, J. R. Mazzeo, J. C. Gebler,  
481 J. H. M. Schellens, H. Rosing and J. H. Beijnen, *J. Am. Soc. Mass Spectrom.*, 2009, **20**,  
482 2021-2033.
- 483 8. C. Atmanene, S. Petiot-Bécard, D. Zeyer, A. Van Dorselaer, V. Vivat Hannah and S.  
484 Sanglier-Cianféroni, *Anal. Chem.*, 2012, **84**, 4703-4710.
- 485 9. A. Konijnenberg, A. Butterer and F. Sobott, *BBA - Proteins and Proteomics*, 2013, **1834**,  
486 1239-1256.
- 487 10. B. T. Ruotolo, J. L. P. Benesch, A. M. Sandercock, S.-J. Hyung and C. V. Robinson, *Nat.*  
488 *Protoc.*, 2008, **3**, 1139-1152.
- 489 11. C. Uetrecht, R. J. Rose, E. Van Duijn, K. Lorenzen, and Albert J. R. Heck, *Chem. Soc.*  
490 *Rev.*, 2010, **39**, 1633-1655.
- 491 12. M. F. Bush, I. D. G. Campuzano, and C. V. Robinson, *Anal. Chem.*, 2012, **84**, 7124-7130.
- 492 13. J. L. Benesch and B. T. Ruotolo, *Curr. Opin. Struct. Biol.*, 2011, **21**, 641-649.
- 493 14. J. Snijder, R. J. Rose, D. Veessler, J. E. Johnson and A. J. R. Heck, *Angew. Chem. Int. Ed.*,  
494 2013, **52**, 4020-4023.
- 495 15. L. Han and B. T. Ruotolo, *Int. J. Ion Mobil. Spectrom.*, 2013, **16**, 41-50.
- 496 16. M. Benassi, Y. E. Corilo, D. Uria, R. Augusti and M. N. Eberlin, *J. Am. Soc. Mass*  
497 *Spectrom.*, 2009, **20**, 269-277.
- 498 17. J. P. Williams, T. Bugarcic, A. Habtemariam, K. Giles, I. Campuzano, P. M. Rodger and P.  
499 J. Sadler, *J. Am. Soc. Mass Spectrom.*, 2009, **20**, 1119-1122.
- 500 18. M. Zhu, B. Bendiak, B. Clowers and H. H. Hill, *Anal. Bioanal. Chem.*, 2009, **394**,  
501 1853-1867.
- 502 19. G. J. Dear, J. Munoz-Muriedas, C. Beaumont, A. Roberts, J. Kirk, J. P. Williams and I.  
503 Campuzano, *Rapid Commun. Mass Spectrom.*, 2010, **24**, 3157-3162.
- 504 20. M. Fasciotti, A. F. Gomes, F. C. Gozzo, B. A. Iglesias, G. F. de Sá, R. J. Daroda, M.  
505 Toganoh, H. Furuta, K. Araki and M. N. Eberlin, *Org. Biomol. Chem.*, 2012, **10**, 8396-8402.
- 506 21. L. Ahonen, M. Fasciotti, G. B. A. Gennäs, T. Kotiaho, R. J. Daroda, R. M. Eberlin and R.  
507 Kostianen, *J. Chromatogr. A*, 2013, **1310**, 133-137.
- 508 22. V. E. Wright, F. Castro-Gómez, E. Jurneczko, J. C. Reynolds, A. Poulton, S. D. R. Christie,  
509 P. Barran, C. Bo and C. S. Creaser, *Int. J. Ion Mobil. Spec.*, 2013, **16**, 61-67.
- 510 23. J. P. Williams, J. M. Brown, I. Campuzano and P. J. Sadler, *Chem. Commun.*, 2010, **46**,  
511 5458-5460.
- 512 24. J. Hofmann, H. S. Hahm, P. H. Seeberger and K. Pagel, *Nature*, 2015, **526**, 241-244.

- 513 25. P. M. Lalli, B. A. Iglesias, H. E. Toma, G. F. Sa, R. J. Daroda, J. C. Silva Filho, J. E.  
514 Szulejko, K. Araki and M. N. Eberlin, *J. Mass Spectrom.*, 2012, **47**, 712-719.
- 515 26. A. Kaufmann, P. Butcher, K. Maden, M. Widmer, K. Giles and D. Uria, *Rapid Commun.*  
516 *Mass Spectrom.*, 2009, **23**, 985-998.
- 517 27. C. Laphorn, T. J. Dines, B. Z. Chowdhry, G. L. Perkins and F. S. Pullen, *Rapid Commun.*  
518 *Mass Spectrom.*, 2013, **27**, 2399-2410.
- 519 28. S. Warnke, J. Seo, J. Boschmans, F. Sobott, J. H. Scrivens, C. Bleiholder, M. T. Bowers, S.  
520 Gewinner, W. Schöllkopf, K. Pagel and G. von Helden, *J. Am. Chem. Soc.*, 2015, **137**,  
521 4236-4242.
- 522 29. R. S. Galaverna, G. A. Bataglion, G. Heerdt, G. F. de Sa, R. Daroda, V. S. Cunha, N. H.  
523 Morgon, M. N. Eberlin, *Eur. J. Org. Chem.*, 2015, **2015**, 2189-2196.
- 524 30. P. M. Lalli, Y. E. Corilo, M. Fasciotti, M. F. Riccio, G. F. de Sá, R. J. Daroda, G. H. M. F.  
525 Souza, M. McCullagh, M. D. Bartberger, M. N. Eberlin and I. D. G. Campuzano, *J. Mass*  
526 *Spectrom.*, 2013, **48**, 989-997.
- 527 31. T. G. Flick, I. D. G. Campuzano and M. D. Bartberger, *Anal. Chem.*, 2015, **87**, 3300-3307.
- 528 32. M. F. Mesleh, J. M. Hunter, A. A. Shvartsburg, G. C. Schatz, and M. F. Jarrold, *J. Phys.*  
529 *Chem.*, 1996, **100**, 16082-16086.
- 530 33. A. A. Shvartsburg and M. F. Jarrold, *Chem. Phys. Lett.*, 1996, **261**, 86-91.
- 531 34. T. W. Knapman, J. T. Berryman, I. Campuzano, S. A. Harris and A. E. Ashcroft, *Int. J. Mass*  
532 *Spectrom.*, 2010, **298**, 17-23.
- 533 35. C. Bleiholder, T. Wyttenbach and M. T. Bowers, *Int. J. Mass Spectrom.*, 2011, **308**, 1-10.
- 534 36. S. E. Anderson, C. Bleiholder, E. R. Brocker, P. J. Stang and M. T. Bowers, *Int. J. Mass*  
535 *Spectrom.*, 2012, **330-332**, 78-84.
- 536 37. C. Bleiholder, S. Contreras, T. D. Do and M. T. Bowers, *Int. J. Mass Spectrom.*, 2013,  
537 **345-347**, 89-96.
- 538 38. C. Bleiholder, S. Contreras and M. T. Bowers, *Int. J. Mass Spectrom.*, 2013, **354-355**,  
539 275-280.
- 540 39. E. G. Marklund, M. T. Degiacomi, C. V. Robinson, A. J. Baldwin and Justin L.P. Benesch,  
541 Collision Cross Sections for Structural Proteomics, *Structure*, <http://impact.chem.ox.ac.uk>,  
542 (accessed May 2015).
- 543 40. D. Guillarme, H. Kim, J. Ruta, H. I. Kim, S. Rudaz, P. V. Johnson, J.-L. Veuthey, L. W.  
544 Beegle, J. L. Beauchamp, W. A. Goddard and I. Kanik, *Anal. Chem.*, 2008, **80**, 1928-1936.
- 545 41. I. Campuzano, M. F. Bush, C. V. Robinson, C. Beaumont, K. Richardson, H. Kim, and H. I.  
546 Kim, *Anal. Chem.*, 2012, **84**, 1026-1033.
- 547 42. C. Laphorn, F. S. Pullen, B. Z. Chowdhry, P. Wright, G. L. Perkins, and Y. Heredia,

548 *Analyst*, 2015, **140**, 6814-6823.

549 43. H. Lavanant, V. Tognetti and C. Afonso, *J. Am. Soc. Mass Spectrom.*, 2014, **25**, 572-580.

550 44. S. A. Stout and C. M. Riley, *Int. J. Pharm.*, 1985, **24**, 193-208.

551 45. TINKER – Software Tools for Molecular Design, <http://dasher.wustl.edu/tinker>, (accessed  
552 January 2015).

553 46. M. J. Frisch, G. W. Trucks, H. B. Schlegel, G. E. Scuseria, M. A. Robb, J. R. Cheeseman,  
554 G. Scalmani, V. Barone, B. Mennucci, G. A. Petersson, H. Nakatsuji, M. Caricato, X. Li, H.  
555 P. Hratchian, A. F. Izmaylov, J. Bloino, G. Zheng, J. L. Sonnenberg, M. Hada, M. Ehara, K.  
556 Toyota, R. Fukuda, J. Hasegawa, M. Ishida, T. Nakajima, Y. Honda, O. Kitao, H. Nakai, T.  
557 Vreven, J. A. Montgomery, Jr., J. E. Peralta, F. Ogliaro, M. Bearpark, J. J. Heyd, E.  
558 Brothers, K. N. Kudin, V. N. Staroverov, R. Kobayashi, J. Normand, K. Raghavachari, A.  
559 Rendell, J. C. Burant, S. S. Iyengar, J. Tomasi, M. Cossi, N. Rega, J. M. Millam, M. Klene,  
560 J. E. Knox, J. B. Cross, V. Bakken, C. Adamo, J. Jaramillo, R. Gomperts, R. E. Stratmann,  
561 O. Yazyev, A. J. Austin, R. Cammi, C. Pomelli, J. W. Ochterski, R. L. Martin, K. Morokuma,  
562 V. G. Zakrzewski, G. A. Voth, P. Salvador, J. J. Dannenberg, S. Dapprich, A. D. Daniels, Ö.  
563 Farkas, J. B. Foresman, J. V. Ortiz, J. Cioslowski, D. J. Fox, Gaussian 09, Revision D.01,  
564 Gaussian, Inc., Wallingford CT, 2009.

565 47. Avogadro – An Open-source Molecular Builder and Visualization Tool,  
566 [http://avogadro.cc/wiki/Main\\_Page](http://avogadro.cc/wiki/Main_Page), (accessed May 2015).

567 48. VMD – Visual Molecular Dynamics, <http://www.ks.uiuc.edu/Research/vmd>, (accessed  
568 January 2015).

569 49. W. Humphrey, A. Dalke and K. Schulten, VMD - Visual Molecular Dynamics, *J. Molec.*  
570 *Graphics*, 1996, **14**, 33-38.

571 50. MobCal – A Program to Calculate Mobilities, <http://www.indiana.edu/~nano/software.html>,  
572 (accessed May 2015).

573 51. MobCalPARSER, <http://sourceforge.net/projects/mobcalparser>, (accessed May 2015).

574 52. Collision Cross Section Database, <http://depts.washington.edu/bushlab/ccsdatabase>,  
575 (accessed February 2015).

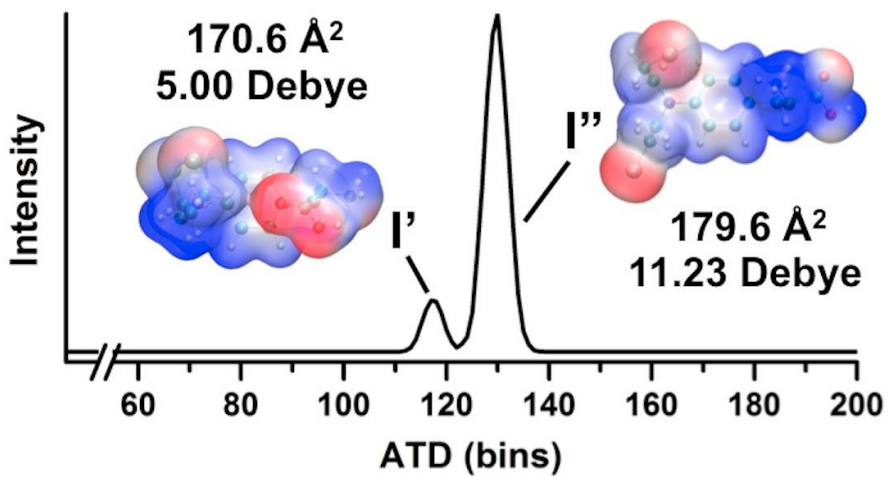
576

577

578 **Figures**

579

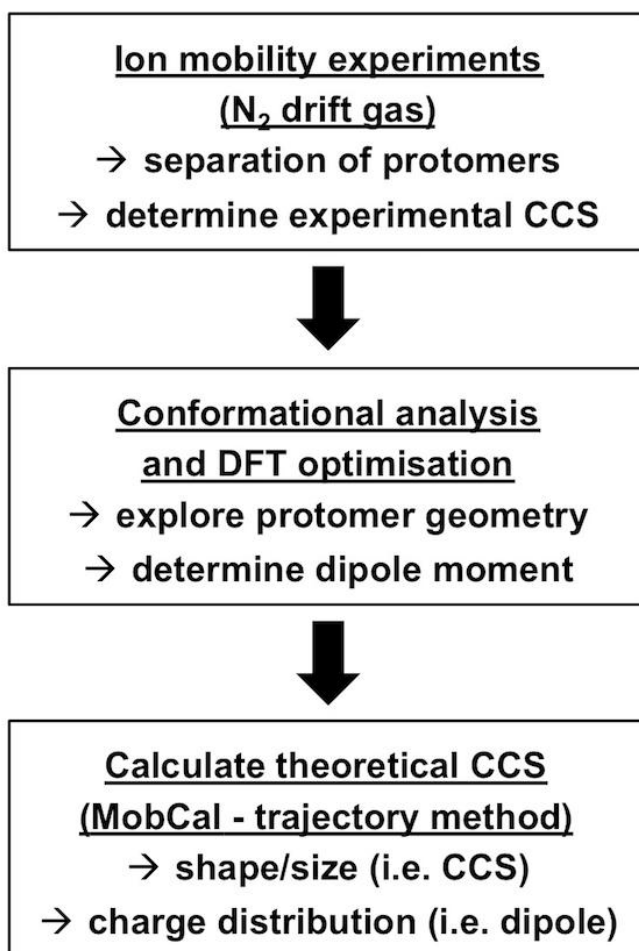
580 Graphical abstract



581

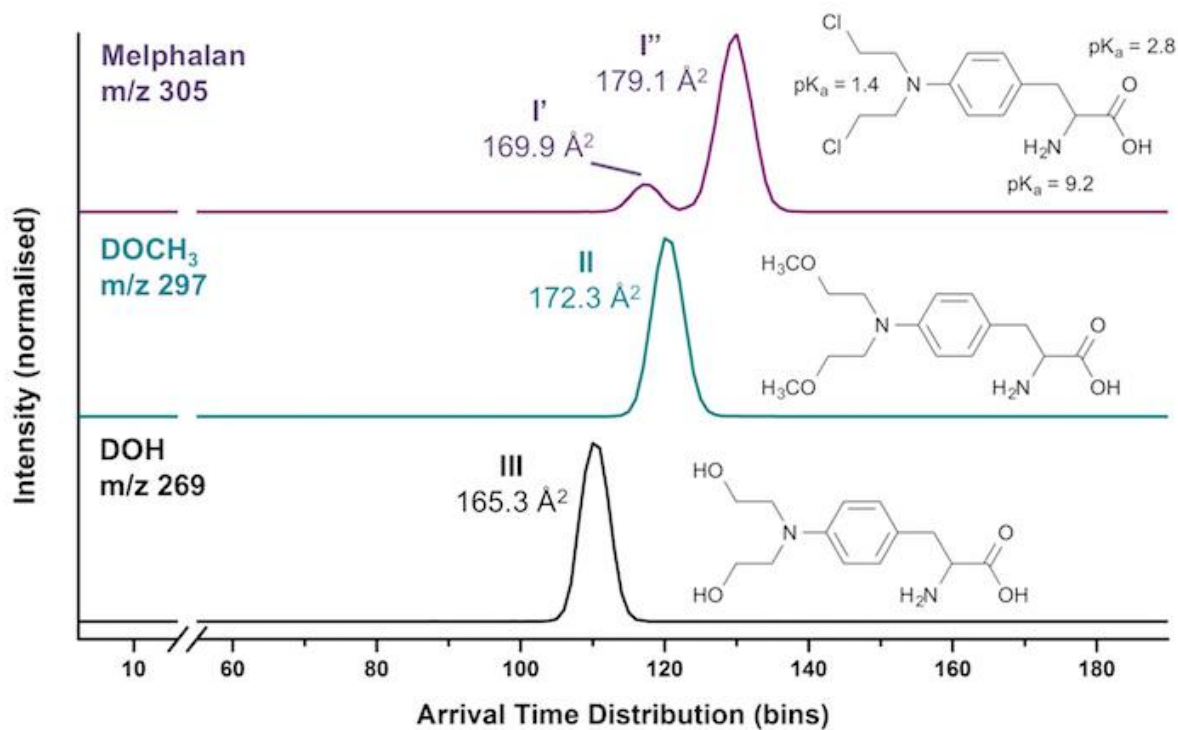
582 Figure 1

583 Overview of the sequence and output of the various experiments and calculations.



584

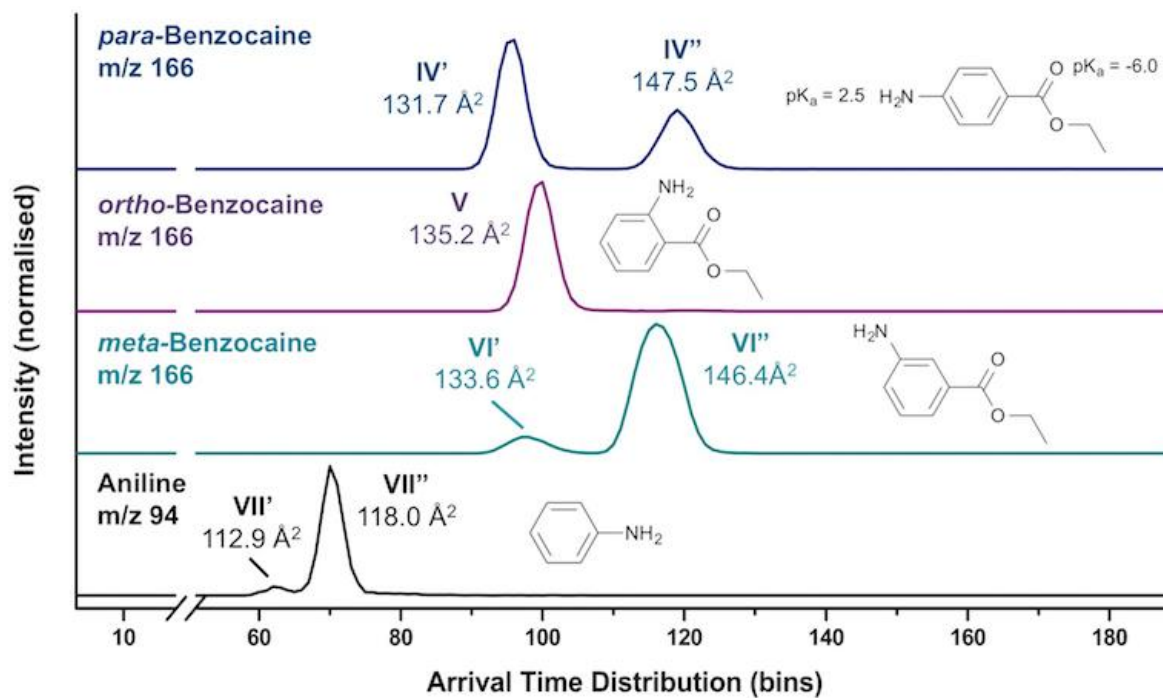
585 Figure 2:  
586 Observation of two peaks for melphalan (I; top panel), but only one peak for the DOCH<sub>3</sub>  
587 (II) and DOH (III) hydrolysis products. The drift time difference between the two  
588 melphalan peaks is larger than the difference between DOH and DOCH<sub>3</sub>.  
589



590  
591  
592

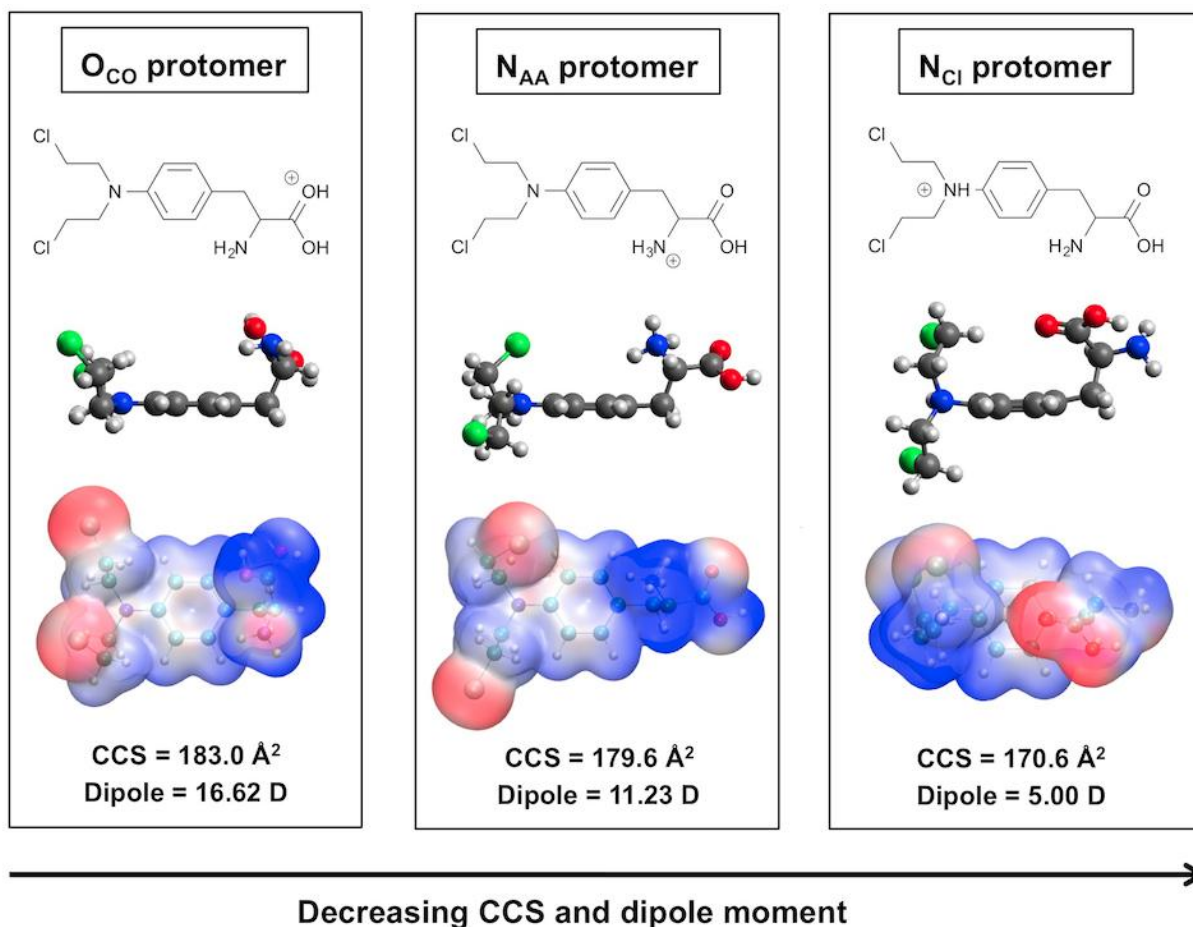
593 Figure 3:  
594 Observation of two peaks for *para*-benzocaine (**IV**) and *meta*-benzocaine (**VI**) as well as  
595 aniline (**VII**). Only one peak is observed for *ortho*-benzocaine (**V**).

596



597

598 Figure 4  
 599 3D-visualisation of the lowest-energy structures of melphalan (I) after conformational  
 600 analysis of the protonated molecules and subsequent standard-level DFT optimisation.  
 601 Three possible protomers are shown: O<sub>CO</sub> (left), N<sub>AA</sub> (center) and N<sub>Cl</sub> (right). Molecular  
 602 electrostatic potentials (MEPs) are also given. Red areas display negative sites (e.g.  
 603 electron dense) and blue areas more positive sites (e.g. protonated).



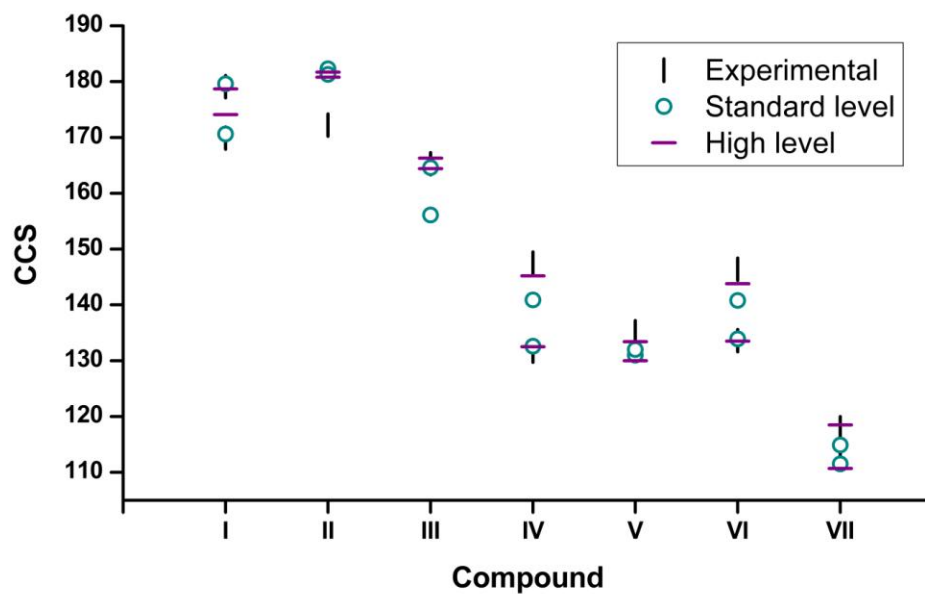
604

605

606 Figure 5

607 Visualisation of the experimental and calculated (both “standard” and “high” level) CCS  
608 values ( $\text{\AA}^2$ ) from Table 2 and 3. Only 4 of the 7 compounds investigated (**I**, **IV**, **VI**, and **VII**)  
609 are separated experimentally into protomer pairs (**I'**/**I''** etc.), while for all of them CCS  
610 values were calculated for the 2 most plausible isoforms.

611

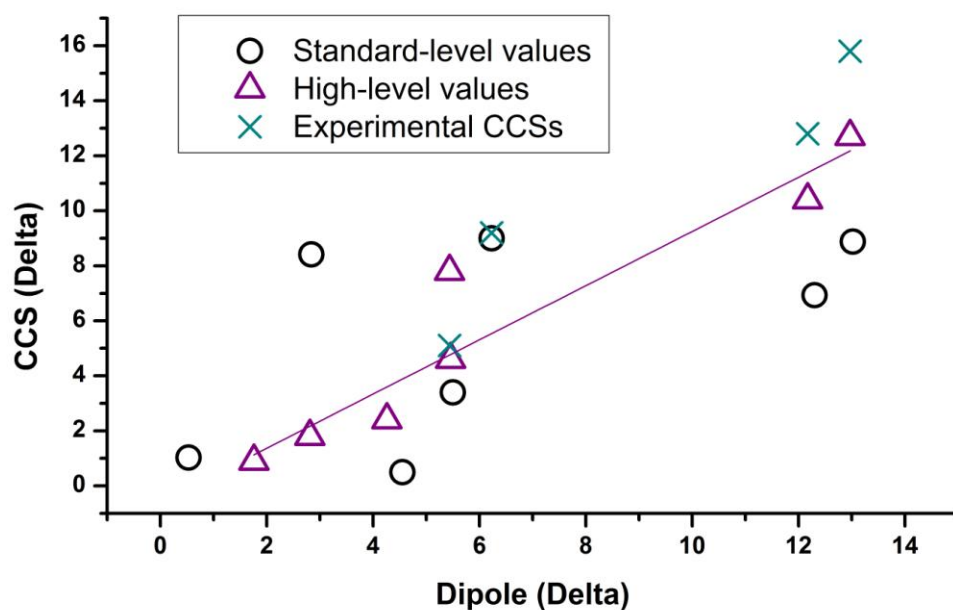


612

613

614

615 Figure 6  
616 Correlation between calculated  $\Delta$ CCS ( $\text{\AA}^2$ ) and  $\Delta$  dipole moment (D) values for protomer  
617 pairs, using “standard” and high-level DFT calculations and the nitrogen-based MobCal  
618 software. For the 4 experimentally observed protomer pairs, the dipole moments were  
619 calculated using the best-fitting DFT level (apart from melphalan, all “high” level). At “high”  
620 level a linear fit ( $R^2=0.8784$ ) suggests itself with aniline as an outlier, while at “standard”  
621 level, many calculated ( $\Delta$ )CCS deviate from the experiment and no correlation is found  
622 with the calculated dipoles ( $R^2=0.1543$ ).  
623



624  
625

626 **Tables**

627

628 **Table 1**

629 Experimental CCS<sub>N2</sub> values derived from TWIMS. MobCal-calculated CCS<sub>N2</sub> using both  
 630 “standard” and high-level DFT optimizations are given for comparison. A detailed  
 631 overview of the calculated values can be found in Tables 2 and 3, together with calculated  
 632 energies, Boltzmann weights and dipole moments.

Analyte	Observed signal(s)	Protonation site	CCS <sub>exp.</sub> (Å <sup>2</sup> )	CCS <sub>calc.</sub> (Å <sup>2</sup> )	
			(Synapt G2 HDMS)	Standard level	High level
Melphalan (Mel)	<b>I'</b>	N <sub>Cl</sub>	<u>169.9 (± 1.5)</u>	<u>170.6</u>	174.1
	<b>I''</b>	N <sub>AA</sub>	<u>179.1 (± 0.9)</u>	<u>179.6</u>	178.7
Dimethoxymelphalan (DOCH <sub>3</sub> )	<b>II</b>	N <sub>OCH<sub>3</sub></sub>	172.2 (± 0.9)	182.3	181.7
		N <sub>AA</sub>		181.3	180.8
Dihydroxymelphalan (DOH)	<b>III</b>	N <sub>OH</sub>	<u>165.3 (± 0.6)</u>	164.6	<u>166.3</u>
		N <sub>AA</sub>		156.1	<u>164.4</u>
<i>para</i> -benzocaine	<b>IV'</b>	O <sub>CO</sub>	<u>131.7 (± 0.8)</u>	132.6	<u>132.5</u>
	<b>IV''</b>	N <sub>NH<sub>2</sub></sub>	<u>147.5 (± 0.6)</u>	140.9	<u>145.2</u>
<i>ortho</i> -benzocaine	<b>V</b>	O <sub>CO</sub>	<u>135.2 (± 0.3)</u>	131.0	<u>131.0</u>
		N <sub>NH<sub>2</sub></sub>		132.0	<u>133.4</u>
<i>meta</i> -benzocaine	<b>VI'</b>	O <sub>CO</sub>	<u>133.6 (± 1.1)</u>	133.9	<u>133.5</u>
	<b>VI''</b>	N <sub>NH<sub>2</sub></sub>	146.4 (± 0.8)	140.8	<u>143.8</u>
Aniline	<b>VII'</b>	ring ( <i>para</i> -)	<u>112.9 (± N/A)</u>	111.5	<u>110.7</u>
	<b>VII''</b>	N <sub>NH<sub>2</sub></sub>	<u>118.0 (± 2.8)</u>	114.9	<u>118.5</u>

Underlined values represent best matching calculated and experimental CCS values

633

634

635 Table 2  
 636 Overview of the 5 lowest-energy melphalan structures for each protomer. Structures were  
 637 acquired after conformational analysis of the protonated molecule, followed by  
 638 standard-level DFT optimization. The global E ranking and energies (relative to the  
 639 lowest-energy structure) give an indication of which protonation sites are most favored in  
 640 the gas-phase. Note the significantly different dipole moments for the N<sub>AA</sub>/O<sub>CO</sub> and N<sub>Cl</sub>  
 641 structures.

Protonation site	E-ranking (relative)	E-ranking (global)	Rel. E (kcal/mol)	Boltzmann weight (%)	Dipole (Debye)	CCS <sub>calc.</sub> (Å <sup>2</sup> )
N <sub>AA</sub> <sup>†*</sup>	<u>1</u>	<u>1</u>	<u>0.0000</u>	<u>10.87</u>	<u>11.23</u>	<u>179.6</u>
	2	2	0.0220	10.47	11.49	177.3
	3	3	0.0878	9.37	11.38	181.0
	4	4	0.1908	7.87	12.66	179.2
	5	5	0.1995	7.76	12.26	176.6
N <sub>Cl</sub>	<u>1</u>	<u>17</u>	<u>1.0718</u>	<u>1.78</u>	<u>5.00</u>	<u>170.6</u>
	2	23	1.2669	1.28	7.55	170.5
	3	30	2.6268	0.13	7.72	170.1
	4	33	3.1156	0.06	4.77	172.4
	5	37	3.6565	0.02	4.70	177.5
O <sub>CO</sub>	<u>1</u>	<u>151</u>	<u>31.0944</u>	<u>0.00</u>	<u>16.62</u>	<u>183.0</u>
	2	152	34.4133	0.00	18.33	182.3
	3	153	34.4195	0.00	18.13	185.6
	4	154	35.4411	0.00	22.65	184.1
	5	155	37.1824	0.00	16.86	181.2

Underlined values represent calculated CCS values for lowest-energy structures

† Expected protonation site in solution (i.e. based on pK<sub>a</sub>)

\* Favoured protonation site in the gas phase (i.e. based on Boltzmann weights)

642

643

644 Table 3  
 645 Overview of the lowest-energy structure for each protomer of dimethoxy- and  
 646 dihydroxymelphalan (DOCH<sub>3</sub> and DOH). Structures were acquired after conformational  
 647 analysis of the protonated molecule and both “standard” and high-level DFT optimization.  
 648 Note that, unlike melphalan, N<sub>AA</sub> is the least favored protomer. Similar dipole moments  
 649 are observed for each protonation site. The global energy ranking is given for each  
 650 compound and per DFT optimization level.

Analyte	Protonation site	DFT opt. level	E-ranking (per level)	Relative E (kcal/mol)	Boltzmann weight (%)	Dipole (Debye)	CCS <sub>TM,N2</sub> (Å <sup>2</sup> )	CCS <sub>exp.</sub> (Å <sup>2</sup> )
Mel (I)	N <sub>AA</sub> <sup>†*</sup>	Standard	1	0.0000	10.87	11.23	179.6	179.1 (± 0.9)
		High	1	0.0000	8.23	10.55	178.7	
	N <sub>Cl</sub>	Standard	17	1.0718	1.78	5.00	170.6	169.9 (± 1.5)
		High	5	0.2027	5.85	5.09	174.1	
DOCH <sub>3</sub> (II)	N <sub>AA</sub> <sup>†</sup>	Standard	126	7.5470	0.00	8.50	181.3	172.2 (± 0.9)
		High	119	5.7718	0.01	9.78	180.8	
	N <sub>OCH3</sub> <sup>*</sup>	Standard	1	0.0000	15.76	7.97	182.3	
		High	1	0.0000	11.98	8.02	181.7	
DOH (III)	N <sub>AA</sub> <sup>†</sup>	Standard	26	4.7214	0.01	3.73	156.1	165.3 (± 0.6)
		High	34	5.3294	0.01	9.80	166.3	
	N <sub>OH</sub> <sup>*</sup>	Standard	1	0.0000	35.99	6.57	164.6	
		High	1	0.0000	36.68	6.99	164.4	

† Expected protonation site in solution (i.e. based on pK<sub>a</sub>)

\* Favoured protonation site in the gas phase (i.e. based on Boltzmann weights)

651

652

653 Table 4  
 654 Overview of the lowest-energy structure for each of the benzocaine and aniline  
 655 protomers, after conformational analysis of the protonated molecule and both “standard”  
 656 and high-level DFT optimization. For all molecules (apart from *ortho*-benzocaine)  
 657 significantly different CCS values are observed for both protomers. Standard-level DFT  
 658 optimization tends to underestimate CCS values, but similar dipole moments are  
 659 observed at both levels anyway.  
 660

Analyte	Protonation site	DFT opt. level	E-ranking (per level)	Relative E (kcal/mol)	Boltzmann weight (%)	Dipole (Debye)	CCS <sub>TM,N2</sub> (Å <sup>2</sup> )	CCS <sub>exp.</sub> (Å <sup>2</sup> )
<i>para</i> -benzocaine (IV)	O <sub>CO</sub> <sup>+</sup>	Standard	1	0.0000	67.22	2.73	132.0	131.7 (± 0.8)
		High	1	0.0000	74.22	2.62	132.5	
	N <sub>NH2</sub> <sup>†</sup>	Standard	5	11.6453	0.00	15.75	140.9	147.5 (± 0.6)
		High	5	11.9007	0.00	15.59	145.2	
<i>ortho</i> -benzocaine (V)	O <sub>CO</sub>	Standard	5	9.9485	0.00	0.99	131.0	135.2 (± 0.3)
		High	3	9.9485	0.00	1.04	131.0	
	N <sub>NH2</sub> <sup>†*</sup>	Standard	1	0.0000	68.58	5.54	131.5	
		High	1	0.0000	74.59	5.30	133.4	
<i>meta</i> -benzocaine (VI)	O <sub>CO</sub> <sup>+</sup>	Standard	1	0.0000	45.62	0.96	133.9	133.6 (± 1.1)
		High	1	0.0000	57.02	0.87	133.5	
	N <sub>NH2</sub> <sup>†</sup>	Standard	5	1.3987	4.30	13.25	140.8	146.4 (± 0.8)
		High	5	2.4900	0.85	13.05	143.8	
Aniline (VII)	ring ( <i>para</i> -) <sup>*</sup>	Standard	1	0.0000	99.22	1.67	111.5	112.9 (± N/A)
		High	1	0.0000	90.60	1.62	110.7	
	N <sub>NH2</sub> <sup>†</sup>	Standard	2	2.9687	0.68	7.18	114.9	118.0 (± 2.8)
		High	2	1.3535	9.36	7.07	118.5	

† Expected protonation site in solution (i.e. based on pK<sub>a</sub>)

\* Favoured protonation site in the gas phase (i.e. based on Boltzmann weights)

661

662

663 Table 5  
 664 Comparison of CCS values calculated for structures with or without their charge  
 665 distribution. Apart from melphalan (I), the effect of the charge distribution is essential in  
 666 order to calculate a distinct CCS for each of the compound's protomers.

Analyte	Protonation site	CCS <sub>calc.</sub> (Å <sup>2</sup> )	
		Charge distr.	No charge distr.
Mel (I)	N <sub>Cl</sub>	170.6	149.0
	N <sub>AA</sub>	179.6	155.9
DOCH <sub>3</sub> (II)	N <sub>OCH3</sub>	181.7	161.8
	N <sub>AA</sub>	180.8	161.5
DOH (III)	N <sub>OH</sub>	166.3	144.4
	N <sub>AA</sub>	164.4	142.0
<i>para</i> -benzocaine (IV)	O <sub>CO</sub>	132.5	109.2
	N <sub>NH2</sub>	145.2	109.4
<i>ortho</i> -benzocaine (V)	O <sub>CO</sub>	131.0	105.2
	N <sub>NH2</sub>	133.4	106.1
<i>meta</i> -benzocaine (VI)	O <sub>CO</sub>	133.5	109.4
	N <sub>NH2</sub>	143.8	108.8
Aniline (VII)	ring ( <i>para</i> -)	110.7	76.6
	N <sub>NH2</sub>	118.5	76.6

667